J. Fluid Mech. (2008), *vol.* 610, *pp.* 43–67.
doi:10.1017/S0022112008002565 Printed in the United Kingdom

The effects of flow stratification by non-cohesive sediment on transport in high-energy wave-driven flows

DANIEL C. CONLEY[1], SILVIA FALCHETTI[2,3], IRIS P. LOHMANN[4] AND MAURIZIO BROCCHINI[5]

[1]Marine Institute, University of Plymouth, Plymouth, UK

[2]NATO Undersea Research Centre, La Spezia, Italy

[3]Dipartimento di Ingegneria delle Costruzioni, dell'Ambiente e del Territorio, Università di Genova, 16145 Genova, Italy

[4]SimCorp A/S, Copenhagen, Denmark

[5]Istituto di Idraulica e Infrastrutture Viarie, Univesità Politecnica delle Marche, Ancona, Italy

(Received 10 July 2007 and in revised form 2 May 2008)

The two-way effects of the time-varying suppression of turbulence by gradients in suspended sediment concentration have been investigated using a modified form of the Generalized Ocean Turbulence Model (GOTM). Field measurements of fluid velocities and sediment concentrations collected under high-energy conditions (mobility number $\approx$900) have been simulated both including and neglecting the feedback between sediment and turbulence. The results show that, when present, this feedback increases the wave-coherent component of transport relative to the mean component of transport, which can even change the direction of transport. Comparisons between measured and simulated time series of near-bed sediment concentrations show great coherence (0.95 correlation) and it is argued that the differences in net transport rates may be partially explained by the use of a uniform grain size in the simulations. It is seen that the effects of sediment stratification scale with orbital velocity divided by sediment setting velocity, u_m/w_s, for all grain sizes.

1. Introduction

Numerous studies (e.g. Gallagher, Elgar & Guza 1998) have highlighted the fact that traditional parametric models of sediment transport under waves cannot be utilized to reliably predict all types of cross-shore transport even on a qualitative basis. While individual models may be able to reproduce either onshore (e.g. Trowbridge & Young 1989) or offshore (e.g. Thornton, Humiston & Birkemeier 1996) bedform translations, no traditional parametric or process-based model is capable of predicting both with a constant set of model parameters (e.g. Plant *et al.* 2004). In order to address this, many recent publications have proposed factors which are not currently accounted for in sediment transport relations. Among the potential explanations proposed are: the effects boundary layer disturbances by through-bed secondary currents (Conley & Inman 1994; Lohmann *et al.* 2006), higher moments of velocity or acceleration (Elgar, Gallagher & Guza 2001) and hypothesized transport affects arising from fluid accelerations (Calantoni & Puleo 2006; Hoefel & Elgar 2003; Nielsen 2006).

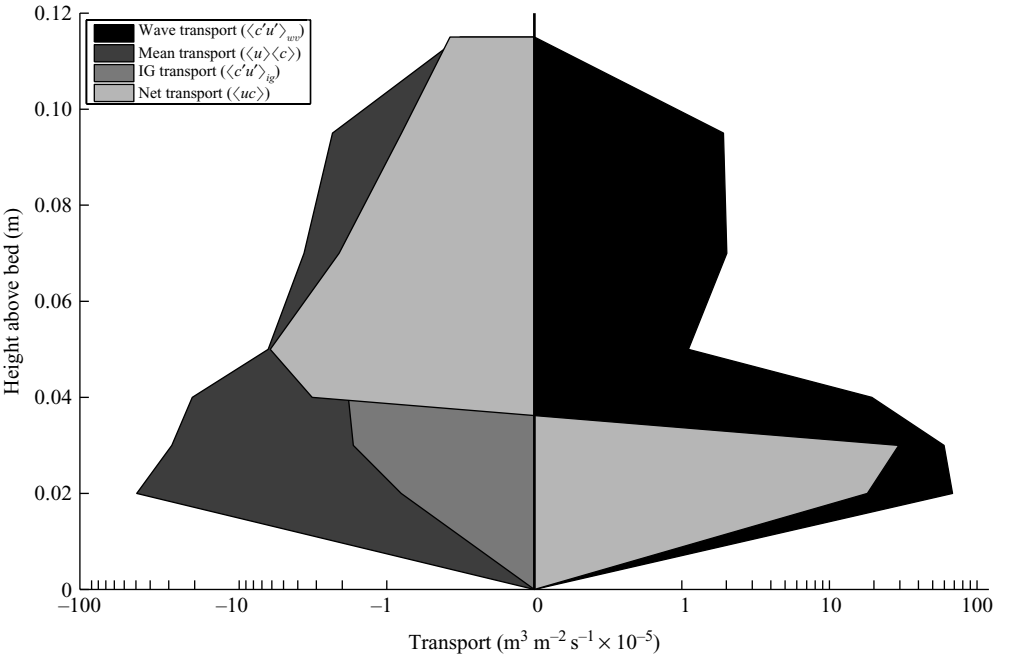

FIGURE 1. Plot of the vertical distribution of mean, wave, infra-gravity, and net sediment transport signals calculated from a 512 s field data sample from the Sandy Duck experiment (Conley & Beach 2003).

Conley & Beach (2003) reported detailed measurements under storm conditions of the sediment load very near the bed. They observed that the vertical profile of net sediment transport could exhibit a reversal in cross-shore transport direction, with an offshore-directed transport high in the water column gradually weakening as the bed is approached and in the bottom few centimetres a complete reversal in direction, with the bottom transport being directed onshore. Ribberink & Al-Salem (1995) also made similar observations in sheet flows generated in an oscillatory flow tunnel. In both cases, this near-bed transport signal was far bigger than the signal higher in the water column and the depth- and time-averaged transport was not infrequently onshore, even in the presence of a net offshore current. When Conley & Beach (2003) examined the frequency distribution of the transport (figure 1), they observed that this vertical pattern was due to a shift in the relative contribution of the wave-coherent transport signal. Far from the sand bed, the largest transport component is the mean component and an offshore mean current results in offshore-directed (negative) net transport. However, as the bed is approached, the wave coherent component of transport begins to dominate. That this component is onshore directed (positive), is not fore-ordained and in fact, standard energetics-based considerations suggest it would be offshore directed if the third moment of wave velocities were negative (offshore). However, in all the observations of Conley & Beach (2003) the wave-coherent component was onshore directed. Other than conditions where strong bedform patterns exist, other investigators have also observed an onshore-directed wave-coherent transport component. An analysis of the phasing of sediment concentration and wave orbital velocities indicates that this onshore component is due to pulses of extremely high

sediment concentrations very near the bed which coincide with the strong onshore-directed orbital velocities under the crest of the wave. These high concentrations quickly settle out to the bed so that they are not available to the mean current for offshore transport and the subsequent high-concentration pulses under the trough are considerably lower. The net effect of these processes is an onshore-directed transport. It is worth noting that this scenario is practically diametrically opposed to the 'suspension event' scenario developed from observations collected in the lower concentration regions farther from the bed (e.g. Hanes 1991). In order to properly explain the total transport signal under waves, the peak shear stresses associated with wave crest velocities may be sufficient to explain the development of the high-concentration pulses, but the failure of current models to predict the onshore transport under these conditions suggests that currently considered phenomena are inadequate to explain the subsequent rapid fall out of the sediment load.

There is a long history associated with the study of the effects of turbulent damping by non-cohesive sediment, starting with the experimental works of Vanoni (1946) and Einstein & Chien (1955) and continuing with theoretical and experimental work to the present day (Cellino & Graf 2007; Coleman 1981; Gelfenbaum & Smith 1986; Hermann & Madsen 2007; Lau & Chu 1987; Lyn 1992; Taylor & Dyer 1977; Winterwerp 2001, 2006). All these studies relate to the effects on turbulent properties and current profiles in essentially time-invariant open channel flows. Some researchers (e.g. Byun & Wang 2005) have reported observing sediment stratification effects on tidal time scales and some works (e.g. McLean 2005) exist regarding the effects of sediment stratification on wave mean sediment profiles. Recent studies of the essentially instantaneous effects of turbulent damping by sediment stratification at time scales less than the surface gravity wave period are seemingly contradictory. From a comparison of one-dimensional turbulence models, Davies *et al.* (1997) deduced that turbulent damping by sediment was unimportant due to similar results of 1-DV turbulence models including and excluding stratification effects. Using the same data, Dohmen-Janssen, Hassan & Ribberink (2001) inferred that turbulence damping was present and was more important for finer sediments. In laboratory experiments of suspensions of fine sediments ($20\,\mu\text{m} < D_{50} < 70\,\mu\text{m}$) under various oscillatory flows, Lamb, D'Asaro & Parsons (2004) reported the clear observation of the development of near-bed high-density sediment layers (HDL) which showed little intra-wave variability. Their observations indicated that the presence of sediment clearly inhibited the near-bed transport of turbulence and resulted in a strongly reduced boundary layer thickness.

The gradient Richardson number (Ri) is often used to suggest whether buoyancy forces due to density gradients are important in stabilizing a shear flow. When Ri for a flow exceeds a critical value, Ri_{crit}, the density gradients are assumed to stabilize the flow and the production of turbulence is diminished. In flows for which the effective fluid density gradients are due to gradients in the concentration of suspended sediment, this turbulent damping leads to a reduction in the diffusion of sediment higher into the water column, thereby maintaining a greater proportion of the sediment load near the bed. Under waves, this increased near-bed sediment load translates into an increased sediment load coherent with the high-velocity flows under the wave crests. Linear stability analysis gives a lower limit for Ri_{crit} of 0.25 (Canuto *et al.* 2001).

Figure 2 shows a typical time-series plot of the vertical distribution of a bulk Richardson number, Ri_b calculated from the field data described in Conley & Beach

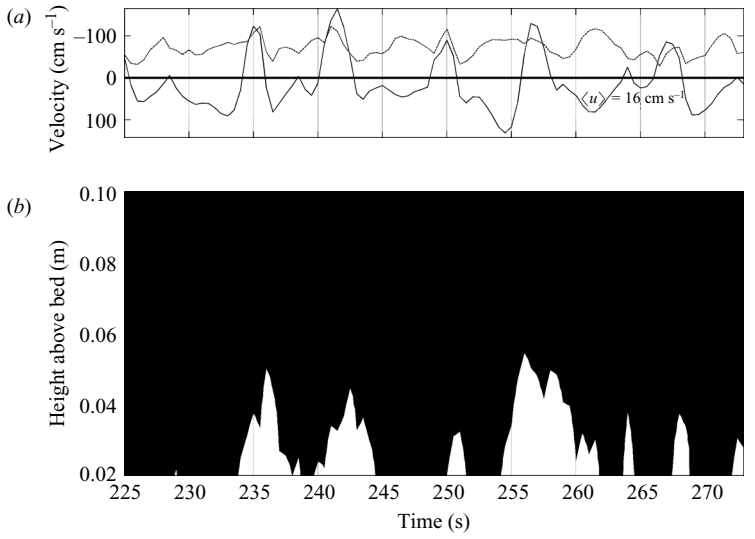

FIGURE 2. Plot of the time history of (*a*) cross-shore velocity (solid line) and longshore velocity (dashed line) and (*b*) the bulk Richardson number calculated for the Sandy Duck field data from figure 1. Richardson number is plotted as two-shade plot where the threshold for the lighter shade is at the linear stability limit of $Ri = 0.25$.

(2003). For this figure, Ri_b was calculated as

$$Ri_b = \frac{-g\partial C/\partial z}{\left[\left(\dfrac{\rho_0\rho_s}{\rho_s - \rho_0}\right) + C\right](\partial u/\partial z)^2} \tag{1}$$

where ρ_0 is the density of water, ρ_s is the bulk density of sediment, C is the sediment concentration expressed as volume/volume and u is the magnitude of the horizontal velocity vector. The velocity shear, $\partial u/\partial z$, was calculated as a mean value over the wave boundary layer and the observed concentrations were smoothed by fitting individual profiles to an exponential form. The results presented in figure 2 suggest that the presence of suspended sediment loads for which turbulence is actively damped is quite common in the energetic field conditions under which these data were gathered. The figure also illustrates that, because the high-concentration pulses are mainly associated with the crests of the waves, the damping of turbulence is highly biased towards periods of onshore flux.

Given these observations, it is hypothesized that the damping of turbulence by sediment in the fluid–sediment boundary layers under high-energy wave conditions is a critical process in determining net sediment transport. This paper reports a series of tests based on numerical modelling of field conditions to examine this hypothesis. In particular these tests will be utilized to examine whether there is a significant difference between wave-driven sediment transport calculated by accounting for or ignoring turbulent damping by sediment and whether the inclusion of turbulent damping can help to reproduce the observed pattern of transport reversals in the water column.

2. Approach

2.1. *Model description*

The base model used for these investigations was the one-dimensional Generalized Ocean Turbulence Model (GOTM) (Burchard, Bolding & Villareal 1999; Umlauf, Burchard & Bolding 2006) which is an open-source FORTRAN-based turbulence model designed specifically to properly simulate phenomena associated with turbulent mixing processes in a column of fluid with density gradients. The model has been developed to be generally applicable and has an extensive list of applications (Blackford, Allen & Gilbert 2004; Ralston & Stacey 2006; Stips *et al.* 2002).

In the one-dimensional vertical profile model solved in GOTM where the horizontal advective terms are neglected, the momentum equations become

$$\left.\begin{aligned} \frac{\partial u}{\partial t} - \frac{\partial}{\partial z}\left[(\nu + \nu_T)\frac{\partial u}{\partial z}\right] &= -g\frac{\partial \eta}{\partial x}, \\ \frac{\partial v}{\partial t} - \frac{\partial}{\partial z}\left[(\nu + \nu_T)\frac{\partial v}{\partial z}\right] &= -g\frac{\partial \eta}{\partial y}, \end{aligned}\right\} \tag{2}$$

where u, v are the horizontal components of fluid velocity in the x (cross-shore) and y (longshore) direction respectively, ν is the kinematic viscosity, ν_T, the eddy viscosity, g is gravity and η is the sea surface elevation. The eddy viscosity used in GOTM includes a stability parameter, c_μ, which in a classic mixing length (L) parameterization (Prandtl 1925) would appear as

$$\nu_t = c_\mu \sqrt{k} L. \tag{3}$$

Here k is the turbulent kinetic energy (TKE) and L is the turbulent mixing length. The use of a stability function in a turbulent closure model (Burchard & Bolding 2001; Canuto *et al.* 2001) serves the purpose of parameterizing the pressure–strain contributions to the Reynolds stress. GOTM includes multiple possibilities for the stability function and although we discuss later what the effect of the different stability functions is, for most of this work we use the most basic, constant, mixing function. The mixing length is, in turn, taken as a function of TKE and the turbulent dissipation, ε, and can be determined from

$$L = \left(c_\mu^0\right)^3 \frac{k^{3/2}}{\varepsilon} \tag{4}$$

where c_μ^0 is taken to be 0.5562. In this work, the k–ε type two-equation turbulence closure model (Rodi 1987) is selected in which the transport equation for TKE is expressed as

$$\frac{\partial k}{\partial t} - \frac{\partial}{\partial z}\left[(\nu_t)\frac{\partial k}{\partial z}\right] = \nu_t M^2 - \mu_t N^2 - \varepsilon \tag{5}$$

with the first two terms on the right representing the shear and buoyancy production respectively. M is the shear frequency, N the Brunt–Väisälä frequency, and μ_t is an eddy diffusivity appropriate for passive tracers commonly assumed equivalent to the diffusivity of heat. M can be expressed as

$$M = \sqrt{\left(\frac{\partial u}{\partial z}\right)^2 + \left(\frac{\partial v}{\partial z}\right)^2} \tag{6}$$

and N as

$$N = \sqrt{\frac{\partial}{\partial z}\left(-g\frac{\rho - \rho_0}{\rho_0}\right)} \tag{7}$$

where ρ is the local density and ρ_0 is the clear water density. The final equation necessary to close the system is the transport equation for dissipation. Including the numerical constants used, this equation is

$$\frac{\partial \varepsilon}{\partial t} - \frac{\partial}{\partial z}\left[(\mu_\varepsilon)\frac{\partial \varepsilon}{\partial z}\right] = \frac{\varepsilon}{k}(1.44\nu_t M^2 + \mu_\varepsilon N^2 - 1.92\varepsilon). \tag{8}$$

As in Burchard, Petersen & Rippeth (1998), the eddy diffusivity for dissipation, μ_ε, is taken as equal to $\nu_t/1.08$. For the current simulations, the constant stability function for momentum (3) is used in which $c_\mu = c_\mu^0 = 0.5562$.

The equation for sediment concentration, C, assumes a classic vertical advection–diffusion form in which the horizontal advective terms are ignored and can be expressed as

$$\frac{\partial C}{\partial t} - \frac{\partial}{\partial z}\left[\mu_s \frac{\partial C}{\partial z}\right] = w_s \frac{\partial C}{\partial z} \tag{9}$$

where w_s is the sediment settling velocity and is positive downward. The relation of Zanke (1977) is utilized to approximate the settling velocity of sediment with a mean grain diameter D:

$$w_s = 10\frac{\nu}{D}\left(\sqrt{1 + \frac{0.01 g D^3(\rho_S - \rho_0)}{\nu^2 \rho_0}} - 1\right). \tag{10}$$

The sediment eddy diffusivity, μ_s, can be expressed as

$$\mu_s = \beta c_\mu^s \sqrt{k} L. \tag{11}$$

A free parameter, β, has been included which represents the mean ratio between the passive tracer diffusivity and the diffusivity of sediment (Nielsen & Teakle 2004). The stability function used for sediment diffusivity, c_μ^s, includes standard Prandtl number dependence

$$c_\mu^s = \frac{c_\mu}{Pr_t^0} \tag{12}$$

where Pr_t^0 is the turbulent Prandtl number for stable conditions (= 0.7143).

The model described here is very similar to those used in many other studies related to wave-driven sediment transport (e.g. Henderson, Allen & Newberger 2004; Holmedal, Myrhaug & Eidsvik 2004). The difference is that in this study the vertical gradient of density is not set to zero. This means that the contributions arising from buoyancy (7) are accounted for. Examining the equations, it is clear that the quantity, N, and, by extension, the effects of sediment stratification, affect both the transport (5) and the dissipation (8) of TKE which, in turn, affects the eddy diffusivity and eddy viscosity both directly, (3), as well as indirectly through the mixing length (4) which also has dissipation dependence.

2.2. *Boundary conditions*

The boundary conditions used for these simulations include no-slip boundary conditions at the bottom and no-stress conditions at the water surface,

$$\left.\begin{aligned} u = v = 0, \qquad & z = -h, \\ (\nu_t + \nu)\frac{\partial u}{\partial z} = (\nu_t + \nu)\frac{\partial v}{\partial z} = 0, \quad & z = 0, \end{aligned}\right\} \tag{13}$$

and similarly, no-flux conditions are utilized for TKE at the upper and lower boundaries, i.e.

$$\nu_t \frac{\partial k}{\partial z} = 0, \quad z = 0, -h. \tag{14}$$

The boundary condition for dissipation is derived by forcing the turbulent length scale definition (4) to match the classical linear behaviour [$L = \kappa(z' + z_0)$] near the bottom boundary, which results in the relation

$$\varepsilon = \left(c_\mu^0\right)^3 \frac{k^{3/2}}{\kappa\,(z' + z_0)}. \tag{15}$$

Here, κ is the von Kármán constant, z' represents the distance from the boundary, and z_0 is the boundary roughness length. As the conditions studied here involve energetic flat bed conditions, it is assumed that the dominant contribution to bed roughness is the sediment load. Roughness length is then calculated as a combination of the time-invariant grain roughness component and the time-varying sediment-load-dependent component which is calculated according to Nielsen (1992). The complete relation is

$$z_0 = 0.03h_0 + 5.67\sqrt{u_*^2 - 0.05g'D}\sqrt{\frac{D}{g'}} \tag{16}$$

where h_0 is the Nikuradse equivalent roughness height, u_* is the bottom friction velocity ($\sqrt{\tau_0/\rho}$), and g' is reduced gravity ($= g(\rho_s - \rho_0)/\rho_0$). GOTM estimates friction velocity by applying the log-layer approximation

$$u_* = \frac{\kappa\sqrt{u^2 + v^2}}{\ln((z + z_0)/z_0)} \tag{17}$$

to a velocity point near the bed which is selected to always be higher than the bed roughness (16).

The sediment boundary condition involves the imposition of a reference concentration, C_0, at the bottom which is related to instantaneous bed stress as expressed by Smith & McLean (1977):

$$C_0 = \gamma\left[\left(\frac{u_*}{u_*^C}\right)^2 - 1\right] \tag{18}$$

where γ is a calibration parameter, and the critical friction velocity, u_*^C, is calculated as

$$u_*^C = \begin{cases} \dfrac{4w_s}{D_*} & \text{for} \quad 1 < D_* \leqslant 10 \\ 0.4w_s & \text{for} \quad D_* > 10. \end{cases} \tag{19}$$

D_*,a normalized grain diameter referred to as the sedimentologic grain diameter, is calculated as

$$D_* = D\left(\frac{g'}{\nu^2}\right)^{1/3}. \tag{20}$$

The Rouse equation is then used to define the Dirichlet boundary condition for the bottom grid cell

$$C(z_1) = C_0\left[\frac{z_1(h-z_0)}{2z_0(h-z_1/2)}\right]^{w_s/\kappa u_*}. \tag{21}$$

A no-flux condition is applied as the top boundary condition for sediment concentration.

In the current work, the momentum equations are forced with point velocity measurements ($u(z_m, t)$, $v(z_m, t)$) which have been recorded at a fixed elevation above the bed (z_m). As discussed by Burchard (1999) the solution method employed is approximately equivalent to specifying the sea surface slope and recreates the measured velocity identically.

2.3. *Calibration and simulations*

The simulations presented here are all based on field measurements which were collected in 1997 as part of the SANDYDUCK experiment and are discussed carefully in Conley & Beach (2003). Most of the results presented here come from simulations forced by a 1024 s velocity time series collected around 04:41 GMT on 19 October. Two components of horizontal velocity were collected using a Marsh-McBirney electromagnetic current meter located 0.35 m above the bed and sediment concentration was estimated from 19 channels of optical backscatter data collected from a fibre optic sensor (FOBS) (Beach, Sternberg & Jonsson 1992) deployed in the bottom 0.50 m of the water column. The significant wave height (H_{sig}) for this period was 1.21 m and the peak period (T_p) was 6.5 s. The simulations were performed for a 2.0 m water depth with D of 0.0002 m. The sediment mobility number, Ψ (Nielsen 1992), is a dimensionless parameter which provides a measure of the balance of forces on sediment in intense flows, and can be written as

$$\Psi = \frac{u_m^2}{(\rho_s/\rho_0 - 1)gD} \tag{22}$$

where u_m is the peak velocity under the wave. For the wave event analysed in this work, the peak velocity is 1.7 m s^{-1}. This means that for 200 μm sand, the mobility number is 893. As the corresponding peak shear velocity is 0.2 m s^{-1}, the wave Shields number for these simulations is 12.3. These values indicate that the conditions being simulated here are clearly flat bed. Other than this, there is nothing special about this time period nor the results produced and the model has been run for hundreds of hours of simulated time, but concentrating on a specific condition helps to focus attention on the contributions of the inclusion of sediment stratification.

In order to perform the simulations the values of free parameters in the model had to be determined. As one goal of this work was to attempt to recreate field observations, the calibration procedure involved matching the simulated and observed mean concentration profiles for the 1024 s time period upon which we concentrate. When performing simulations in which the two-way feedback between sediment load and flow is included, the best match between observed and calculated mean concentration is found with $\gamma = 1.54 \times 10^{-3}$ and setting $\beta = 0.55$. This value of γ is the value originally proposed by Smith & McLean and the reduction in sediment

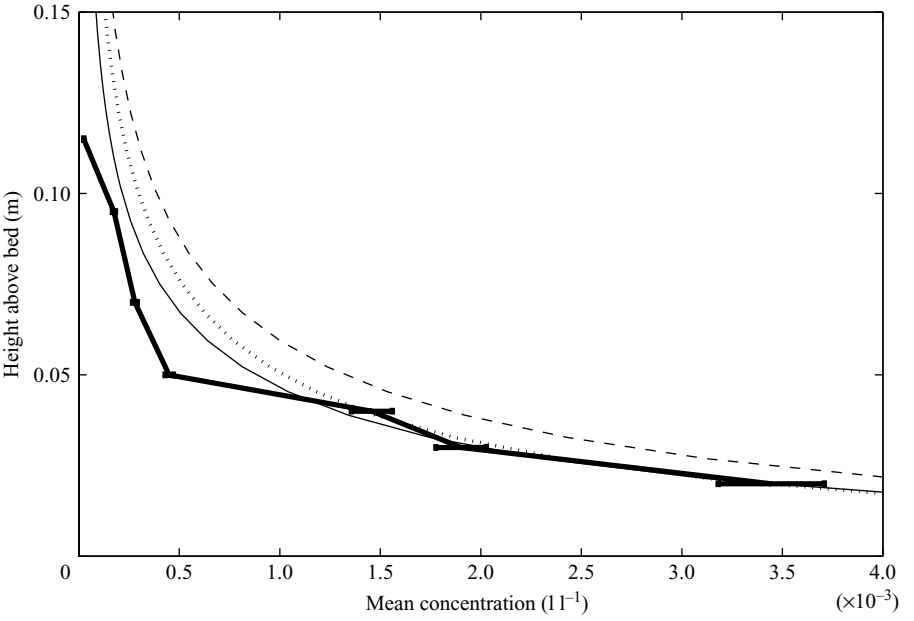

FIGURE 3. Plot of mean concentration profiles. Thin solid line represents best match for simulations accounting for sediment stratification ($\gamma = 1.54 \times 10^{-3}$, $\beta = 0.55$), dotted line is best fit without ($\gamma = 1.2 \times 10^{-3}$, $\beta = 0.55$) and dashed line is simulation without stratification but using parameters derived from stratification results. Thick solid line represents field observations and horizontal bars are the 95 % confidence intervals based on sample variances.

diffusivity is remarkably similar to that obtained by Dohmen-Janssen *et al.* (2001). Observed and simulated mean concentration profiles using these values are presented in figure 3 and as can be seen the match is quite good. However, when simulations are performed without the two-way interaction (dashed line in the figure), the simulated mean concentrations are systematically higher than observations (figure 3). This observation derives from the well-known phenomenon that bed stress is higher for sediment-free flows (e.g. Thompson *et al.* 2006).

In order to eliminate spurious results which occur merely because of the comparison of lower concentration flows with higher concentration flows, we created a second set of calibration coefficients to provide model-data match where the two-way feedback is not included. In these simulations, we are forcing with velocity, not pressure gradient. In the light of this and considering the extra energy which is expended generating turbulence in the case with two-way feedback, it is evident that γ must be adjusted in order to obtain similar concentrations in the two types of simulations. What is less clear is why the β parameter ought to vary between the two simulations. For parametric models, Nielsen & Teakle (2004) have suggested a functional dependence between concentration gradient and the ratio of eddy viscosity to eddy diffusivity, but in the simulations discussed here we are explicitly accounting for the role of concentration gradients in momentum exchange. Thus, in order to avoid double accounting as well as to minimize the number of adjustable parameters, it was decided to leave β constant. For this reason, when a match between simulated and observed sediment concentrations is desired, the values of $\gamma = 1.2 \times 10^{-3}$ and $\beta = 0.55$ are used for simulations without two-way feedback (dotted line, figure 3). With these

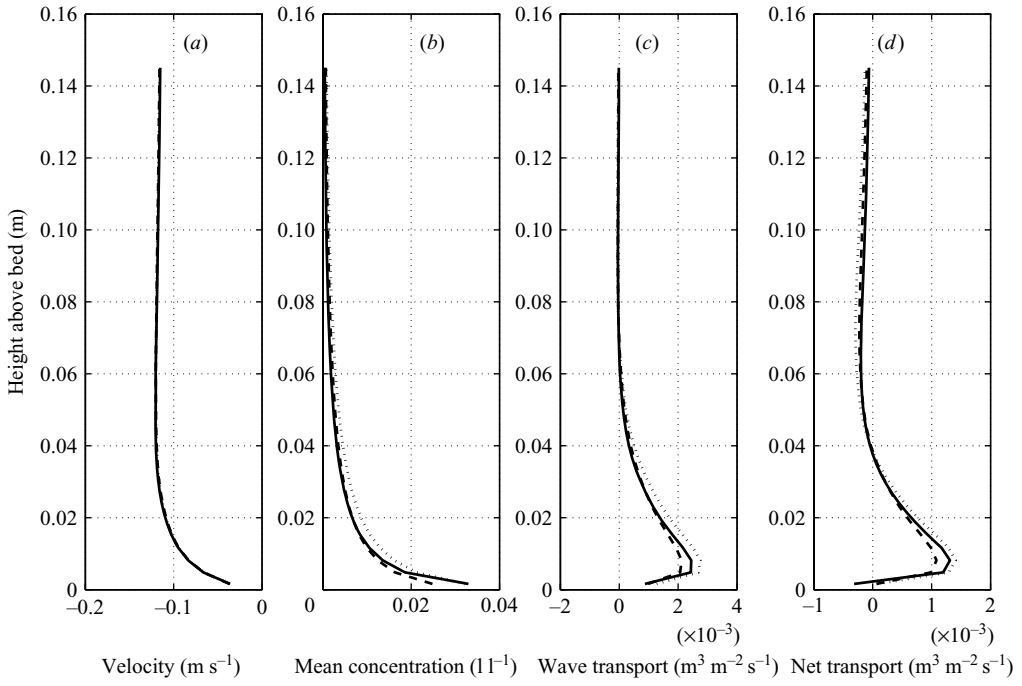

FIGURE 4. Comparisons of profiles of (*a*) mean cross-shore velocity, (*b*) sediment concentration (*c*), wave-coherent cross-shore transport, and (*d*) net cross-shore transport. The three different line types represent: simulation with stratification effects (solid line), simulation without the effects of stratification using the same model parameters as the stratification case (dotted line) and simulation without stratification with the same sediment profile as the stratified case (dashed line).

two sets of parameters it is now possible to proceed with an examination of the effects of including the feedback between sediment concentration and turbulent production in a model of sediment suspension beneath waves.

3. Results

3.1. *Medium sand conditions*

Figure 4 presents profiles of the mean velocity, mean concentration, and mean net and mean wave components of cross-shore transport for three different simulations where the mean is calculated over a wave group of 40 s duration. The three different cases presented are: sediment stratification (two-way density feedback) accounted for (case 1, solid line); sediment stratification ignored with same model parameters as case 1 (case 2, dotted line); and sediment stratification ignored with adjusted model parameters (case 3, dashed line). The figure demonstrates that the inclusion of stratification has essentially no effect on the velocity profile. As previously seen in figure 3, the effect on the sediment concentration is, however, quite large (figure 4*b*) with sediment stratification resulting in systematically lower concentrations for simulations with the same parameter set but similar concentrations when the non-stratified case uses a reduced γ.

The profiles of the wave coherent transport component (in this case calculated as the difference between net and mean transport) are presented in figure 4(*c*). When

comparing the two simulations with the same mean concentration profiles, we can see that the results from the case including stratification are significantly larger than the case which ignores it. In fact when expressed as a percentage of the integrated mean transport signal, the wave component of transport exhibits a 23% increase from the unstratified case ($Q_{wv} = 0.82\, Q_{mn}$) to the stratified case ($Q_{wv} = 1.02\, Q_{mn}$). While, in absolute terms, the unstratified case using the same model parameters as the stratified case appears to exhibit a larger wave component, this is merely a function of the higher total sediment concentrations. In this case, the wave component represents the same 77 % of the mean component of transport as the stratified case with lower concentrations. This figure emphasizes that the two-way feedback between concentration and turbulent generation/dissipation tends to enhance the coherence between peak velocities and the near-bed sediment concentrations.

The effect of all this can be seen in figure 4(*d*) where the profiles of net transport are presented. While the wave component of transport dominates near the bed (below 4 cm) in all cases, its dominance is greater in the simulations including stratification. The second effect of stratification is also evident higher in these profiles (>6 cm) where the sediment stratified case exhibits lower net transport than either of the other two cases. This reduction is due to turbulent suppression in the near-wall high-concentration-gradient region which leads to lower amounts of sediment further from the bed thereby reducing the mean transport component. For the specific 40 s case presented here, the magnitude of the depth-integrated net transport for the stratified case is less than 12 % of either of the non-stratified cases and, more significantly, it is a net onshore transport in contrast to the net offshore transport in the other two cases. This result is not at all general and simulations accounting for sediment stratification can indeed have a net offshore transport, but what is general is that the wave coherent component is enhanced and that the net transport (difference between two larger quantities) is therefore significantly reduced in magnitude.

These differences are evident in figure 5 which presents results for a single wave example taken from the middle of the 1024 s simulation. Figure 5(*a*) provides a graph of the reference velocity as well as the bottom shear velocities for the two cases with stratification and no stratification with the modified model parameters. The shear velocities calculated in GOTM are scalar quantities directly proportional to the bottom shear rate. The key point of this graph is that the shear velocities for the two cases are essentially equal. Figure 5(*b*) shows a grey-scale plot of the sediment load for the stratification case. This plot highlights the behaviour which leads to a net onshore transport near the bed, even in the case of mean offshore velocities. This transport is the product of the strong correlation between high concentrations under the wave crest (see time 1086 s) and the onshore velocities. The friction velocity trace in figure 5(*a*) demonstrates that this correlation is strongly due to the quadratic response between sediment reference concentration and the friction velocity (18). The results presented in figure 5(*c*), where the difference in sediment concentration between the stratified and non-stratified case is plotted, clearly indicate that this behaviour is amplified by the effects of stratification. It is evident from this figure that the near-bed concentrations below approximately 4 cm are increased for the stratified case and that this increase is highest precisely during the periods of highest near-bed concentration, i.e. under the crest of the wave. The net effect of this process is to increase the wave coherent component of transport precisely as observed in figure 4.

It is also clear from this figure that above about 6 cm the concentrations are reduced in comparison to the non-stratified case. Unlike the near-bed concentrations,

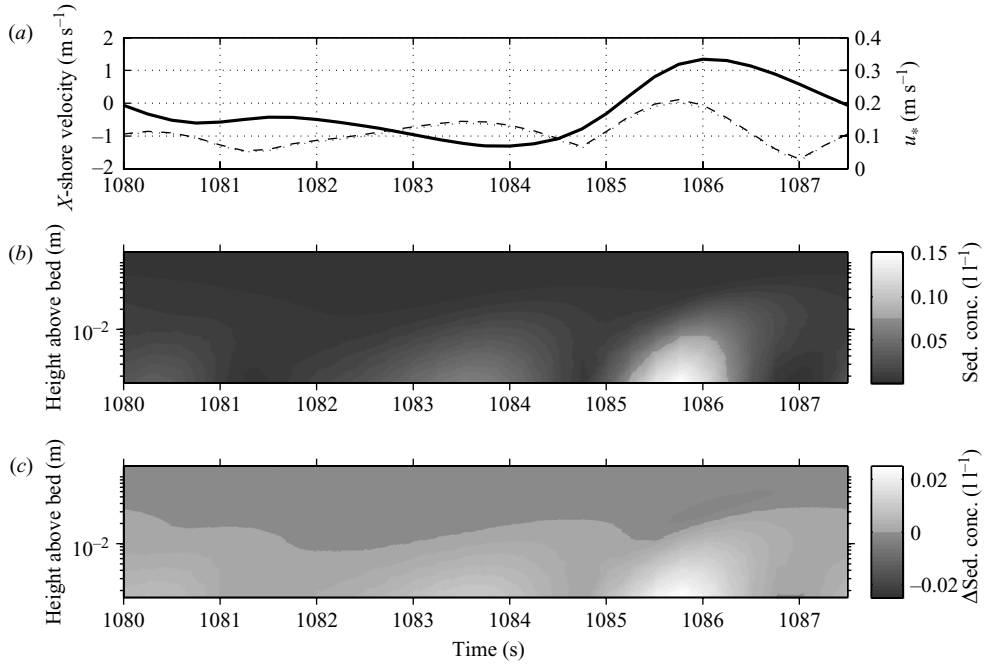

FIGURE 5. Results from single wave event. (*a*) Time history of wave reference velocity (solid line) which serves as forcing and the model friction velocity (dashed line). (*b*) Sediment concentration distribution for the stratified case. (*c*) The difference (stratified – not stratified).

this reduction exhibits little or no time variation so that the net effect is a reduction in the mean transport, again as observed in figure 4. Taken together, these observations illustrate the combined effects of momentary stratification of the water column by sediment suspended from the bottom. Sediment is mobilized off the bottom by the wave action and is diffused into the water column by turbulence. The buoyancy term (7), which results from the density gradient between higher concentration fluid near the bed and lower concentration fluid above, leads to a decrease in the production of turbulence (5) and an increase in dissipation as described by equation (8), all of which results in a reduction in the diffusivity of sediment ((3), (4), (11)) and hence lower concentrations of sediment higher in the water column. However the equal friction velocities in the two cases indicate that the same amount of sediment is mobilized in both cases. As less of this sediment is diffused higher into the water column it is trapped near the bottom where it can quickly respond to the time-varying character of the wave action and amplify the wave coherent transport.

This behaviour is confirmed in figure 6 where the eddy diffusivity profiles at various points during the wave cycle are presented for both the stratified and unstratified case. At all periods and for all elevations the diffusivity is seen to be reduced for the stratified case and this reduction, near the bed, is strongest during the period of peak friction velocity (and hence reference concentration) at 5.75 s. An analysis of the source of this change is difficult to perform due to the temporal evolution of effects. However, it is observed that TKE, dissipation and shear production terms are all reduced in the stratified case. The only quantity which shows a positive change is the buoyancy production. An increase in buoyancy production results in an increase in dissipation (8) and a reduction in TKE (5). Thus, since diffusivity is essentially a ratio

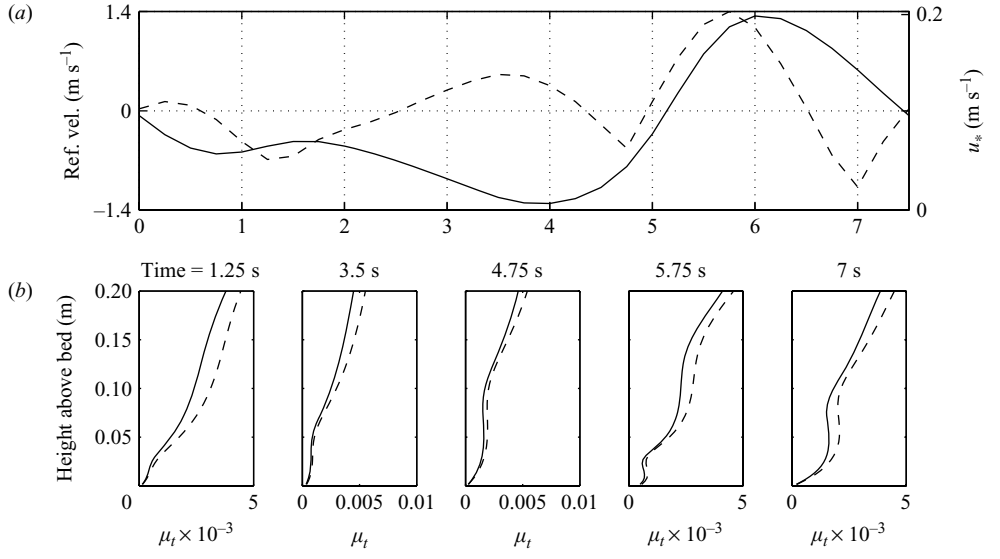

FIGURE 6. Plot illustrating the effect of sediment stratification on eddy diffusivity. (*a*) The wave reference velocity (solid line) and friction velocity (dashed line) and (*b*) profiles of eddy diffusivity at different times. The solid lines represent the cases which include sediment stratification and the dashed lines those without.

of TKE^2/dissipation, this change in buoyancy production clearly drives a reduction in diffusivity.

3.2. *Different grain sizes*

The simulations presented up to now contain model parameters which were selected (calibrated) to reproduce observed conditions. As the observations utilized here are from a single location, there are no results for other grain sizes and we cannot properly calibrate for simulations of different grain sizes. Nonetheless, it is still useful to perform simulations in which all parameters but the grain size are kept constant because comparisons between such results with and without stratification provide a qualitative illustration of the grain size dependence of these effects. For that purpose, we present results from two different sets of simulations, one in which the grain size is reduced from 200 μm to 64 μm, and a second set where it is increased to 600 μm.

The results in figure 7 are derived from the single wave event presented in figure 5 but this time for the very fine sand grains of 64 μm. Two particular features of this simulation can be readily seen in this figure. From the cross-shore velocity results (figure 7*b*) it appears that there is almost a two-layer structure in the velocity profiles with a typical boundary layer structure present in the bottom 0.06 m of the water column with velocities increasing monotonically from the bed. However, at the top of this layer there is a subsequent reduction in velocities (consider for example times 1080.5 s and 1086 s) and a secondary boundary layer structure above that which then evolves into the free stream. This structure is typical of layered stratified flows in which the flow in each layer is partially decoupled from the other. The appropriateness of this analogy is confirmed by figure 7(*c*) where the sediment load in suspension is presented. The initial impression of the figure emphasizes the wave coherent component of suspension, but closer inspection illustrates that all the sediment suspension is constrained to this thin near-bottom layer. This is true not just

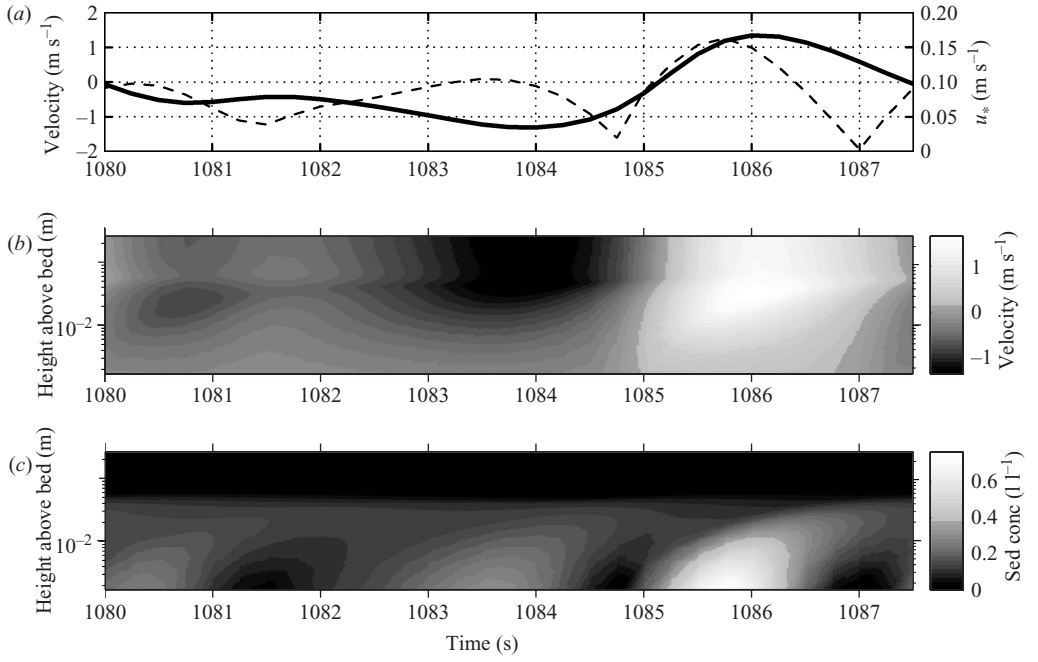

FIGURE 7. Single wave results for same event as in figure 5 but with sediment grain size of 64 μm. (*a*) Time history of wave reference velocity (solid line) which serves as forcing and the model friction velocity (dashed line). (*b*) Fluid cross-shore velocities for the stratified case and (*c*) sediment concentration distribution for the stratified case.

for the near-bed high-concentration burst which is in phase with the friction velocity, but also the diffusive tongues of concentration which propagate with phase up into the flow. In fact, the figure gives the impression that the water column is essentially devoid of sediment at all times at heights greater than approximately 0.07 m above the bed.

These results can be confirmed by considering the averaged profiles for the wave event that are presented in figure 8. The double boundary layer structure can be seen quite clearly in the mean velocity profile in figure 8(*a*) where an inflection point is located at approximately 0.06 m. This layer structure is also observed in the mean concentration profile where the presence of two logarithmic layers is evident, with one existing above an apparent lutocline at approximately 0.05 m. The other dominant feature of this figure is the dramatic total reduction in sediment concentrations for the stratified case, where sediment is practically absent above 0.08 m yet almost constant in the simulations without stratification. This result highlights that the presence of high sediment concentrations leads to a radical reduction in the diffusion of sediment into the water column by strongly diminishing the turbulent kinetic energy in the water column (figure 8*e*). While the observed difference between net and wave transport indicates that the mean component is dominant in both cases (figure 8*c*), the maintenance of the dynamic suspension processes in the layer below the lutocline leads to the seemingly anomalous development of an offshore wave coherent transport component. Reference, however, to figure 7(*c*) demonstrates that this is due to the diffusive sediment plume structure which in the stratified case is trapped below the lutocline. Note that, in this fine sediment case, the net effects of stratification have been a dramatic reduction in total transport (Q_{net} for the unstratified case is 45

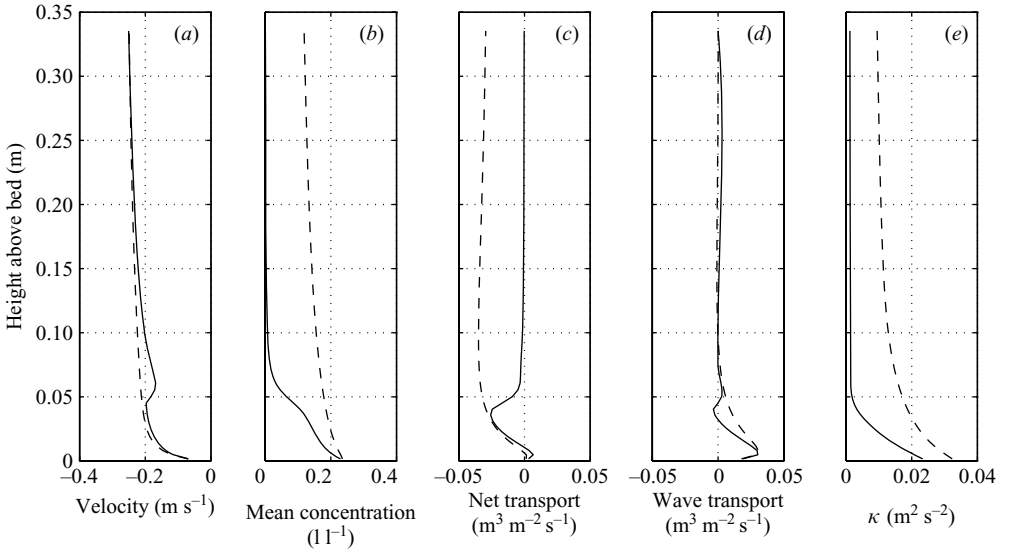

FIGURE 8. Comparisons of profiles of (*a*) mean cross-shore velocity, (*b*) sediment concentration, (*c*) net cross-shore transport, (*d*) wave coherent cross-shore transport, and (*e*) turbulent kinetic energy for simulations using a grain size of 64 μm. The two different line types represent simulation with stratification effects (solid line) and simulation without the effects of stratification (dashed line).

times greater than for the stratified case) and the creation of a high-concentration layer which exhibits a lutocline for an upper boundary through which practically no turbulence passes.

The results for the coarser sediment grain size of 625 μm (figure 9) are much less dramatic, and changes in net transport are inseparable from changes in the quantity of sediment in suspension. This is not surprising considering that in either case, sediment concentration is essentially zero at elevations higher than 0.05 m and that the wave-coherent transport is by far the dominant component (Q_{wave} is approximately 3 times Q_{mn}).

4. Discussion

4.1. *Stratification effect threshold*

The effects of sediment stratification are clearly most important for cases in which the sediment load is great and concentration gradients are strong. In order to observe a case in which the effects of sediment stratification are negligible, we have simulated several wave events of lower intensity. A wave group recorded at 12:01 on 18 October 1997 has been identified as an example of a limit case. The peak current observed during this 21 s group was 0.7 m s^{-1} and the peak shear velocity was 0.075 m s^{-1}. Thus the mobility number was 151 and the Shields parameter was 1.7. The mean concentration and net transport traces are presented in figure 10. While there is a trivial difference in mean concentrations between the simulation with stratification and that without, it should be recalled that these simulations were run with exactly the same sediment parameters. When this is contrasted with the equivalent results in figure 4, it clearly demonstrates how weak the stratification effects are for this case.

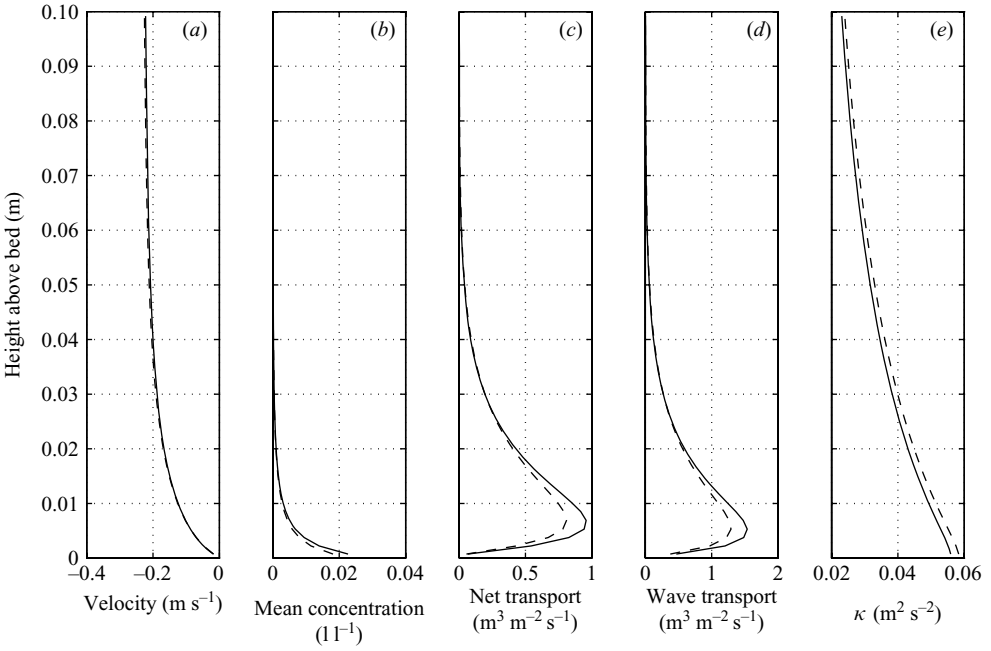

FIGURE 9. As figure 8 but for simulations using a grain size of 625 μm. The solid lines represent simulations with stratification effects and the dashed lines represent simulations without the effects of stratification.

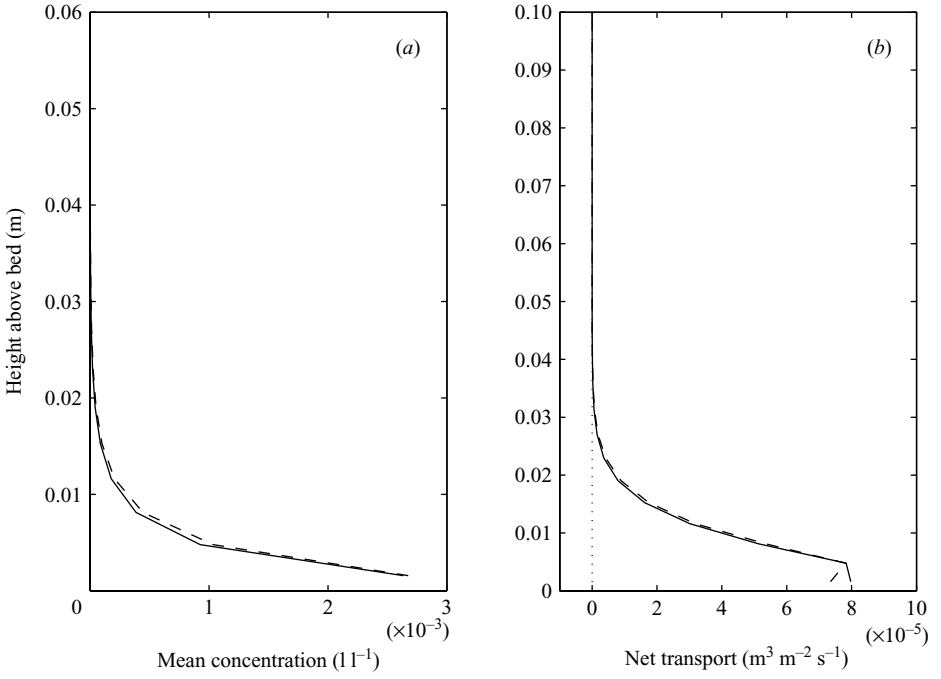

FIGURE 10. Profiles of (*a*) mean concentration and (*b*) net cross-shore transport for simulations of 21 s weaker condition wave group (mobility number = 151, Shields parameter = 1.7). Solid line shows results using sediment stratification and dashed line results omitting stratification. Compare to figure 4 results and consider that both simulations used identical sediment transport parameters ($\gamma = 1.54 \times 10^{-3}$, $\beta = 0.55$).

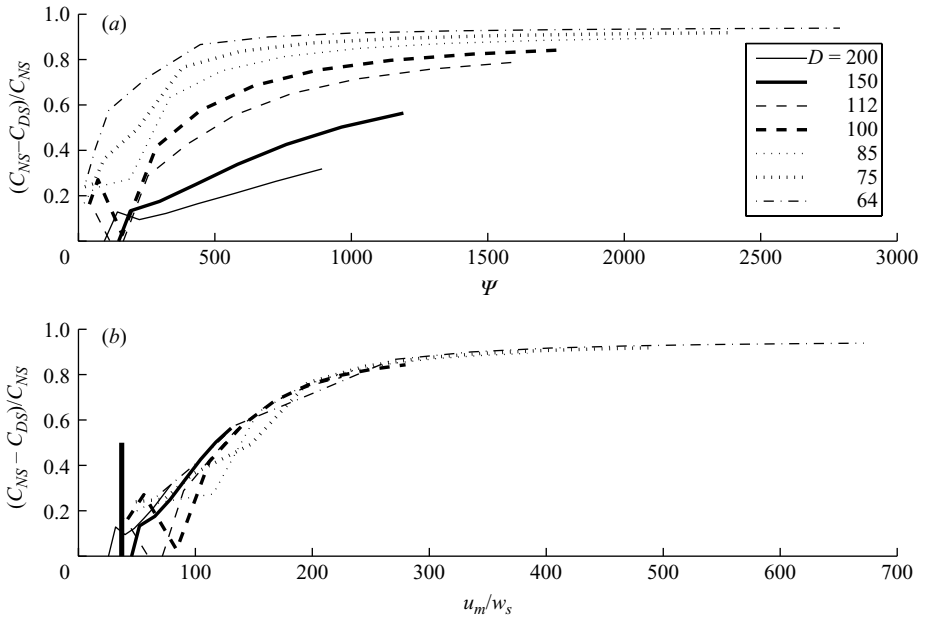

FIGURE 11. Plots of the sediment stratification as represented by ΔC (23) as a function of (*a*) mobility number and (*b*) normalized orbital velocity. The individual lines represent different grain diameters, D, used in the simulation. The solid vertical bar in (*b*) marks the zero crossing of the mean results for all grain sizes.

This observation is corroborated by the comparison of net transport rates in which the only observable difference occurs in the bottom most computational cell.

In order to test whether this result could be considered general or holds only for the sediments utilized, a series of simulations based on the conditions in figure 5 have been performed. This was done by linearly reducing the velocities from the original conditions by a constant factor and running the model. The process was repeated for progressively smaller velocities until the threshold velocity was no longer exceeded and the entire process was replicated for a range of grain sizes from 65 to 200 microns. In order to quantify the effects of stratification, we defined the parameter ΔC as

$$\Delta C = \frac{C_{NS} - C_{DS}}{C_{NS}} \tag{23}$$

where C_{DS} (C_{NS}) represents the sediment load integrated from the bed to 1 m above it for the simulations including (excluding) sediment stratification. This parameter has the quality that it asymptotes to 1 as stratification becomes important and tends towards zero as the importance subsides. At lower velocities, the model-derived values of this function are not well behaved because they represent the ratio of very small quantities in which counterbalancing effects compete. Nonetheless, the general trends are quite clear. The magnitude of the stratification effect has been plotted as a function of mobility number in figure 11(*a*) with each line representing a separate grain size. This figure indicates that not only is the magnitude of the stratification effect different for every grain size but it appears that there are different onset values for each grain size.

Nielsen (1979) presented observations of apparent sediment diffusivities, derived from sediment concentration measurements over ripples, as a function of normalized orbital velocity (u_m/w_s). In these results, he observed a sudden drop in diffusivity

following a range of steadily increasing values and this behaviour was observed at the same u_m/w_s for a wide range of grain diameters. Nielsen (personal communication) suggests that this behaviour may have been due to the common onset of turbulent suppression by sediment stratification. With this proposal in mind, the results presented in figure 11(*a*) have been replotted in figure 11(*b*) where the stratification effect is given as a function of the normalized orbital velocity. The collapse of the results in this figure is quite dramatic and confirms that the effects of stratification are a function of the normalized orbital velocity. The heavy vertical line in figure 11(*b*) marks the zero crossing of the mean of the results for all grain sizes. This occurs at a value of 37 which is higher than the value of 20 suggested by Nielsen's (1979) experimental results but these results are from flat bed conditions and it is likely that turbulence-generated effects would be retarded relative to ripple conditions.

4.2. *Stability function dependence*

The utilization of stability functions (3), (11), (12) is designed to explicitly increase or decrease mixing in the presence of stable or unstable stratification. These functions are of increasing importance with the increasing magnitude of the Richardson number (Ri) and GOTM, which is particularly designed for application in stratified conditions, includes four different stability function schemes. The most basic form is the constant-parameter version which we have employed throughout this work. Additional forms which are available include the Munk & Anderson (1948), the Schumann & Gerz (1995) and the Eifler & Schrimpf (1992) stability functions. In a form which is equivalent to (12), the Munk & Anderson function can be expressed as

$$c_\mu^S = \begin{cases} \dfrac{c_\mu^0}{Pr_t^0}\dfrac{(1+10Ri)^{1/2}}{(1+3.33Ri)^{3/2}} & \text{for } Ri \geqslant 0 \\ \dfrac{c_\mu^0}{Pr_t^0} & \text{for } Ri < 0. \end{cases} \tag{24}$$

The implementation of Schumann & Gerz stability function takes the form

$$c_\mu^S = \frac{c_\mu^0}{\left(Pr_t^0 \mathrm{e}^{-Ri/0.25Pr_t^0} - \dfrac{Ri}{0.25}\right)} \tag{25}$$

and the Eifler & Schrimpf function can be expressed as

$$c_\mu^S = \frac{0.5}{Pr_t^0}\sqrt{1-Ri_f} \tag{26}$$

where Ri_f is the flux Richardson number and can be related to Ri by

$$(1-Ri_f) = \left[\left(\frac{0.5}{Pr_t^0}Ri+1\right)^{0.5} - \frac{0.5}{Pr_t^0}Ri\right]^2. \tag{27}$$

In order to assess the importance of the stability function, the single wave simulation was recalculated four times utilizing each of these stability functions. The mean sediment load and transport results from these simulations are presented in figure 12. As would be expected, the figure illustrates that the results from the simulations utilizing the constant-parameter stability function are those in which the effects of stratification are minimized. While the differences between the different simulations may appear small, the relative contribution of the wave component of transport

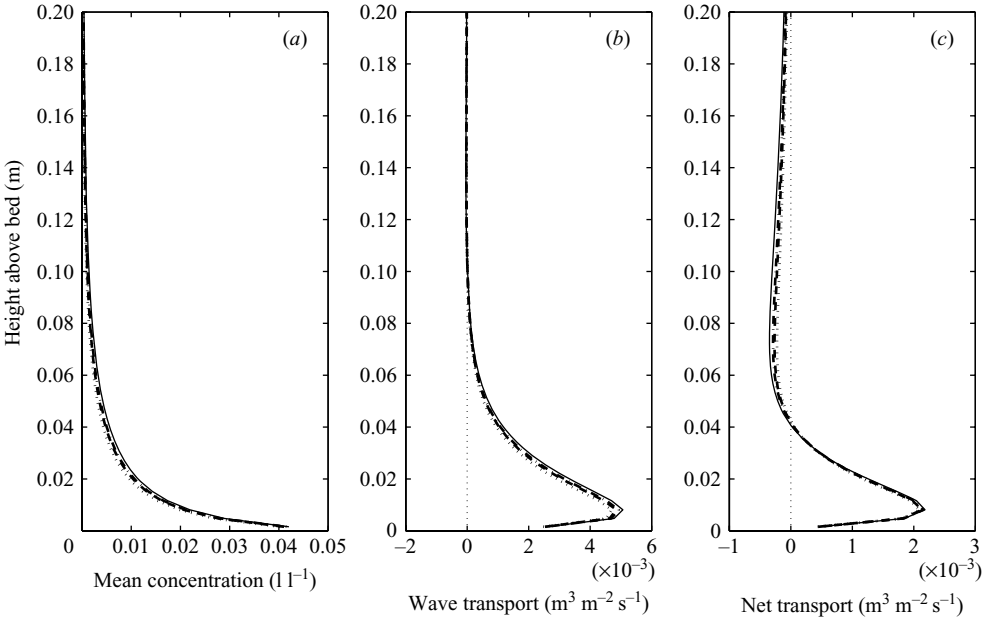

FIGURE 12. Profiles of (*a*) mean concentration, (*b*) wave coherent transport, and (*c*) net cross-shore transport for simulations of single wave events using four different stability functions. Solid line shows constant-parameter results, dashed line Munk & Andersen, dotted line Schumann & Gerz and the dashed-dotted line the results using the Eifler and Schrimpf stability function.

increases by 15 % relative to the mean transport between the constant-parameter case (92 %) and the Schumann & Gerz (107 %) results. This is a large enough difference to change the sign of the net transport direction. While the selection of the appropriate stability function to be used for these simulations is beyond the scope of the current study, it is to be emphasized that the function utilized in the current work is that which minimizes the effects of stratification.

4.3. *Comparison to observations*

While the main goal of this work is primarily to examine how the inclusion of two-way feedback between suspended sediment and the fluid flow which leads to its suspension affects the results of simulations of sediment suspension, a secondary objective is to relate these results to field observations of the process. Other than to constrain model free parameters, the simulation results have not yet been compared to field data but to do so may show how representative the simulations are and indicate where there are weaknesses. Unfortunately a perfect comparison cannot be performed because while relatively good measurements with reasonable coverage in both time and altitude exist for concentration measurements (Conley & Beach 2003), reliable velocity estimates are available at only one or two elevations in the water column. Therefore, in order to be able to compare the simulations and observations, we propose to compare simulated and pseudo-observed transport signals. This is done by performing a GOTM simulation in which the observed velocities at a single elevation are used to force the model. GOTM is structured such that the observed velocity is identically reproduced. The vertical distribution of simulated transport is then calculated as the product of the simulated concentrations and simulated velocities at the same

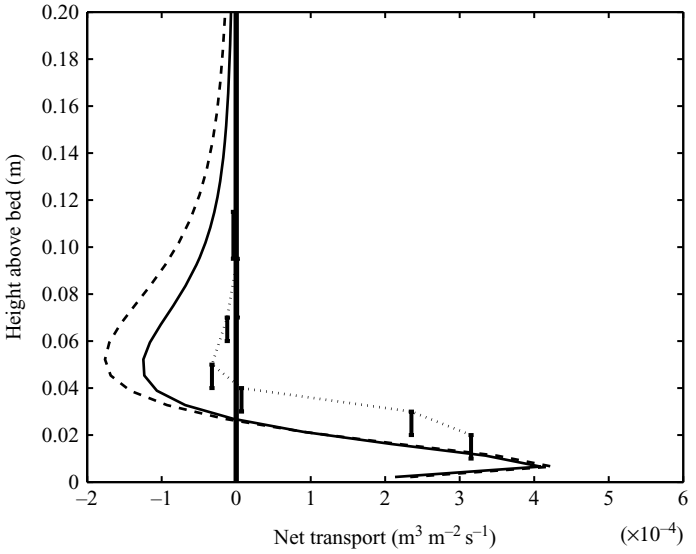

FIGURE 13. Comparison of mean net cross-shore transport as calculated from: observed data (dotted line), simulations with the effects of sediment stratification (solid line), and simulations without stratification (dashed line). Vertical bars on observed transport line represent vertical location uncertainty in the field measurements. The observed transport is calculated using observed concentrations and simulated velocity profiles.

levels. The pseudo-observed transport is calculated as the product of the observed concentrations and the simulated velocities at the corresponding elevations. A further step has been performed to remove potential field data noise for an intervening section of the data in which visual inspection suggests possible contamination of the optical sensors by floating debris (observed during collection). Thus of the 1024 s data we are considering, a 256 s patch was omitted from the following analysis.

Figure 13 is a plot of the vertical distribution of net transport rates for the pseudo-observations (dotted), for simulations including the effects of sediment stratification (solid), and for simulations neglect sediment stratification (dashed). In this figure, the net rate is calculated as the temporal mean of transport over the entire 768 s utilized. There are several observations to be made about this figure. The first is that the observed onshore transport persists somewhat higher (0.04 m above the bottom) than the simulated transport (0.025 m above the bottom). While the vertical locations of the observed concentrations cannot be identified any more accurately than the separation between discrete sensors (Conley & Beach 2003), even taking this into account, it still appears that the onshore transport dies out closer to the bed in the simulations. This is not true for the elevation of the transport minimum (offshore maximum), however, which is approximately the same (0.05 m above the bottom) for observations and simulations. The second point is that the offshore transport appears to be grossly over-estimated in all the simulations. This is reflected in the fact that the simulated depth-integrated net transport is either strongly (no stratification) or weakly (stratified) offshore directed while the observed net transport is distinctly onshore directed. Nonetheless, the ratio between onshore and offshore transport is clearly better reproduced by the stratified case than the unstratified.

In order to begin to understand where the differences between observations and simulations arise, we shall make a comparison of the observed and simulated

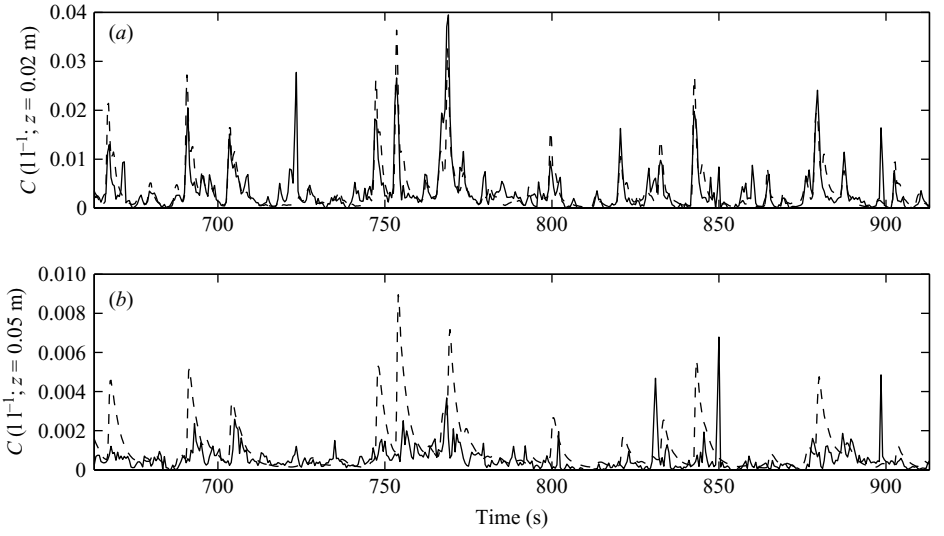

FIGURE 14. Comparison of simulated (dashed) and observed (solid) sediment concentrations at (*a*) 0.02 m and (*b*) 0.05 m. The correlation coefficient between the time series at the lower elevation is 0.76 and 0.35 at the higher elevation.

sediment concentrations. A subsection of the time series for simulated and observed concentrations at two different elevations (0.02 m and 0.05 m) is presented in figure 14(*a*) and 14(*b*) respectively. At the lower station, the two time series are very similar. The mean concentrations are the same for both time series which is not surprising given the fact that model free parameters were adjusted to achieve this end. More impressive is the fact the correlation coefficient between the two time series is 0.76. Nonetheless some differences can be observed in the figure. The most striking is that the observed time series exhibits sporadic high-concentration peaks that are completely absent in the simulations. If we combine this observation with the fact that the means of the two time series are equivalent, this suggests that the lower concentrations for the simulated time series are higher than the observed values. This is quantitatively confirmed by examining the means of the 25 % lowest concentrations for each time series. As suggested by this observation, the mean of the lowest 25 % of simulated concentrations is 2.3 times greater than in the case of the observed concentrations.

The comparison of simulated vs. observed concentrations at the higher elevation (figure 14*b*) differs in that the simulated concentrations are clearly higher than observed (as suggested by figure 3) but the general coherence between the two signals is quite evident. The amplitude mismatch, the increased relative importance of unsimulated high-concentration peaks (e.g. $\sim$850 and 900 s) and the lower signal to noise ratio results in a lower correlation (0.35). The correlations for all seven observation elevations are presented in table 1 and visual inspection of all the signals indicates general coherence at all levels but reduced correlations as a result of the factors discussed above.

While the differences described here may appear trivial and correlations between observations and estimations of these magnitudes might be considered a satisfactory result in many numerical simulations, the effect of these differences on net transport under waves is quite large. As seen in figure 13, the presence of these differences leads

Elevation (m)	0.02	0.03	0.04	0.05	0.07	0.095	0.115
Correlation	0.76	0.41	0.22	0.35	0.26	0.24	0.27

TABLE 1. Correlation between simulated and observed concentrations at the seven observation elevations.

not only to errors in the magnitude of transport but also results in miscalculation of the sign of the depth-integrated transport. With this consideration in mind, it is clear that identifying and rectifying the source of such errors is of high priority.

One potential explanation for the weaknesses in the current simulations is suggested by examining the observations related to stratification effects for different grain sizes which were discussed earlier. The results presented in figure 11 make it clear that, for a given orbital velocity (constant u_m), the effects of stratification are much greater for finer grains (lower w_s). This makes it highly likely that the effects of stratification would be much greater for bottom sediments which contain a distribution of grain sizes than for the single grain size studied here. The presence of a sediment component significantly finer than the mean diameter would result in stratification effects significantly stronger than that predicted based on a single grain size. The qualitative effect of this would be a relative enhancement of the wave-coherent component of transport and a strong reduction in the mean transport component higher in the water column. These changes are precisely those required to make the current simulations more closely approach observations (figure 13). When considering figure 14, it should be clear that further reducing diffusivity might reduce the mean lower concentrations; it is difficult to imagine how stratification would lead to the peaks of higher concentration observed in the data and absent in the simulations. A more probable explanation is that these higher peaks are due to non-diffusive sediment entrainment processes which have been discussed or observed by many authors (e.g. Chang & Scotti 2006; Foster, Beach & Holman 2006) but have not been accounted for in the current simulations.

5. Conclusions

Estimations of bulk Richardson numbers from field data under energetic wave conditions indicate that sediment stratification affects turbulent properties at time scales which are shorter than the wave period. A wave-resolving, 1-DV, coupled turbulence and sediment advection diffusion model (GOTM) has been run in order to investigate the importance of accounting for the time-varying two-way interactions between fluid and sediment (sediment stratification) in terms of cross-shore sediment transport. The model was forced with field measurements from high-energy conditions (mobility number $O(900)$, Shields number $O(12)$) and simulations were performed both including and neglecting sediment stratification effects. The results show that, for medium sands, the inclusion of stratification tends to increase sediment concentrations near the bottom and reduce concentration further from the bed and this effect is time varying and in-phase with the sediment concentration itself. The net effect of this behaviour is an increase in the wave-coherent component of transport relative to the mean component of transport.

Qualitatively, the behaviour does not appear scalable under natural conditions with finer sands developing a lutocline type behaviour that dramatically suppresses the development of turbulence and suspension of sediment outside the bottom

boundary layer. The inclusion of stratification with coarser sediments in which there is little suspension has little qualitative effect. Nonetheless, when the effects of stratification are properly normalized, it is shown that the effects for all grain sizes display a common dependence on orbital velocity normalized by grain settling velocity.

Comparisons of time series of field measurements of near-bed sediment concentrations and simulations show great coherence (0.76 correlation) but relatively large discrepancies between measured and simulated transport rates. Nonetheless, simulations including stratification effects better reproduce the relative transport contributions.

It is shown that the selection of turbulent stability functions has some quantitative effect on the simulations and that the basic function used in these simulations minimizes the relative enhancement of the wave-coherent component of sediment transport.

The authors would like to express their appreciation to Peter Nielsen for his illuminating suggestions and to the anonymous reviewers for their contributions towards improving the manuscript. The ONR Coastal Dynamics program funded the work under which data utilized in this manuscript was collected. Much of the work presented here was performed while the first author was employed at the NATO Undersea Research Facility.

REFERENCES

Beach, R. A., Sternberg, R. W. & Jonsson, R. 1992 A fiber optic sensor for monitoring suspended sediment. *Mar. Geol.* **103**, 513–520.

Blackford, J. C., Allen, J. I. & Gilbert, F. J. 2004 Ecosystem dynamics at six contrasting sites: a generic modelling study. *J. Mar. Systems* **52** (1–4), 191–215.

Burchard, H. 1999 Recalculation of surface slopes as forcing for numerical water column models of tidal flow. *Appl. Math. Modelling* **4**, 737–755.

Burchard, H. & Bolding, K. 2001 Comparative analysis of four second-moment turbulence closure models for the oceanic mixed layer. *J. Phys. Oceanogr.* **31**, 1943–1968.

Burchard, H., Bolding, K. & Villareal, M. R. 1999 *GOTM, a general ocean turbulence model. Theory, implementation and test cases. Tech Rep* EUR 18745-EN, European Commission, JRC Ispra, pp. 1–103.

Burchard, H., Petersen, O. & Rippeth, T. P. 1998 Comparing the performance of the Mellor-Yamada and the k-epsilon two-equation turbulence models. *J. Geophys. Res.* **103** (C5), 10543–10554.

Byun, D.-S. & Wang, X. H. 2005 The effect of sediment stratification on tidal dynamics and sediment transport patterns. *J. Geophys. Res.* **110**, C03011.

Calantoni, J. & Puleo, J. A. 2006 Role of pressure gradients in sheet flow of coarse sediments under sawtooth waves. *J. Geophys. Res.* **111**, C01010.

Canuto, V. M., Howard, A., Cheng, Y. & Dubovikov, M. S. 2001 Ocean turbulence. Part I: One-point closure model-momentum and heat vertical diffusivities. *J. Phys. Oceanogr.* **31** (6), 1413–1426.

Cellino, M. & Graf, W. H. 2007 Sediment-laden flow in open-channels under noncapacity and capacity conditions. *J. Hydraul. Engng* **125** (5), 455–462.

Chang, Y. S. & Scotti, A. 2006 Turbulent convection of suspended sediments due to flow reversal. *J. Geophys. Res.* **111**, C07001.

Coleman, N. L. 1981 Velocity profiles with suspended sediment. *J. Hydraul. Res.* **19**, 211–229.

Conley, D. C. & Beach, R. A. 2003 Cross-shore sediment transport partitioning in the nearshore during a storm event. *J. Geophys. Res.* **108** (C3), 10. doi:1029/2001JC001230

Conley, D. C. & Inman, D. L. 1994 Ventilated oscillatory boundary layers. *J. Fluid Mech.* **273**, 262–284.

Davies, A. G., Ribberink, J. S., Temperville, A. & Zyserman, J. A. 1997 Comparisons between sediment transport models and observations made in wave and current flows above plane beds. *Coast. Engng* **31** (1–4), 163–198.

Dohmen-Janssen, C. M., Hassan, W. N. & Ribberink, J. S. 2001 Mobile-bed effects in oscillatory sheet flow. *J. Geophys. Res.* **106** (C11), 27103–27115.

Eifler, W. & Schrimpf, W. 1992 ISPRAMIX, a hydrodynamic program for computing regional sea circulation patterns and transfer processes. *Tech. Rep.* EUR 14856, European Commission Joint Research Center, Ispra, Italy.

Einstein, H. A. & Chien, N. 1955 *Effects of heavy sediment concentration near the bed on velocity and sediment distribution.* University, of California, Institute of Engineering Research, Berkeley, California, pp. 1–98.

Elgar, S., Gallagher, E. L. & Guza, R. T. 2001 Nearshore sandbar migration. *J. Geophys. Res.* **106** (C6), 11623–11627.

Foster, D. L., Beach, R. A. & Holman, R. A. 2006 Turbulence observations of the nearshore wave bottom boundary layer. *J. Geophys. Res.* **111**, C04011.

Gallagher, E. L., Elgar, S. & Guza, R. T. 1998 Observations of sand bar evolution on a natural beach. *J. Geophys. Res.* **103** (C2), 3203–3215.

Gelfenbaum, G. & Smith, J. D. 1986 Experimental evaluation of a generalized suspended-sediment transport theory. In *Shelf Sands and Sandstones* (ed. R. J. Knight & J. R. McLean). Canadian Society of Petroleum Geologists, Calgary, Alberta, Canada, pp. 133–144.

Hanes, D. M. 1991 Suspension of sand due to wave groups. *J. Geophys. Res.* **96** (C5), 8911–8915.

Henderson, S. M., Allen, J. S. & Newberger, P. A. 2004 Nearshore sandbar migration predicted by an eddy-difusive boundary layer model. *J. Geophys. Res.* **109**, C06024.

Hermann, M. J. & Madsen, O. S. 2007 Effect of stratification due to suspended sand on velocity and concentration distribution in unidirectional flows. *J. Geophys. Res.* **112**, C02006.

Hoefel, F. & Elgar, S. 2003 Wave-induced sediment transport and sandbar migration. *Science* **299**, 1885–1887.

Holmedal, L. E., Myrhaug, D. & Eidsvik, K. J. 2004 Sediment suspension under sheet flow conditions beneath random waves plus current. *Cont. Shelf Res.* **24** (17), 2065–2091.

Lamb, M. P., D'Asaro, E. & Parsons, J. D. 2004 Turbulent structure of high-density suspensions formed under waves. *J. Geophys. Res.* **109**, C12026.

Lau, Y. L. & Chu, V. H. 1987 Suspended sediment effect on turbulent diffusion. *22nd IAHR Congress, Lausanne, Switzerland.*

Lohmann, I. P., Fredsoe, J., Sumer, B. M. & Christensen, E. D. 2006 Large eddy simulation of the ventilated wave boundary layer. *J. Geophys. Res.* **111**, C06036.

Lyn, D. A. 1992 Turbulence characteristics of sediment-laden flows in open channels. *J. Hydraul. Engng* **118** (7), 971–988.

McLean, S. R. 2005 On the calculation of suspended load for noncohesive sediments. *J. Geophys. Res.* **97** (C4), 5759–5770.

Munk, W. H. & Anderson, E. R. 1948 Notes on the theory of the thermocline. *J. Mar. Res.* **3**, 276–295.

Nielsen, P. 1979 *Some Basic Concepts of Wave Sediment Transport*. Series Paper no. 20, Institute Hydrodynamics & Hydraulic Engineering, Technical University Denmark, Lyngby, pp. 1–166.

Nielsen, P. 1992, *Coastal Bottom Boundary Layers and Sediment Transport*. World Scientific.

Nielsen, P. 2006 Sheet flow sediment transport under waves with acceleration skewness and boundary layer streaming. *Coast. Engng* **53** (9), 749–758.

Nielsen, P. & Teakle, I. A. L. 2004 Turbulent diffusion of momentum and suspended particles: A finite-mixing-length theory. *Phys. Fluids* **16** (7), 2342–2348.

Plant, N. G., Holland, K. T., Puleo, J. A. & Gallagher, E. L. 2004 Prediction skill of nearshore profile evolution models. *J. Geophys. Res.* **109**, C01006.

Prandtl, L. 1925 Bericht über Untersuchungen zur ausgebildeten Turbulenz. *Z. Angew. Math. Mech.* **5**, 136–139.

Ralston, D. K. & Stacey, M. T. 2006 Shear and turbulence production across subtidal channels. *J. Mar. Res.* **64** (1), 147–171.

Ribberink, J. S. & Al-Salem, A. A. 1995 Sheet flow and suspension of sand in oscillatory boundary layers. *Coast. Engng* **25**, 205–225.

Rodi, W. 1987 Examples of calculation methods for flow and mixing in stratified flows. *J. Geophys. Res.* **92**, 5305–5328.

Schumann, U. & Gerz, T. 1995 Turbulent mixing in stably stratified shear flows. *J. Appl. Met.* **34**, 33–48.

Smith, J. D. & McLean, S. R. 1977 Spatially averaged flow over a wavy surface. *J. Geophys. Res.* **82** (12), 1735–1746.

Stips, A., Burchard, H., Bolding, K. & Eifler, W. 2002 Modelling of convective turbulence with a two-equation k-e turbulence closure scheme. *Ocean Dyn.* **52** (4), doi. 10.1007/s10236-002-0019-2, 153–168.

Taylor, P. A. & Dyer, K. R. 1977 Theoretical models of flow near the bed and their implications for sediment transport. In *Marine Modeling. The Sea* (ed. E. D. Goldberg), pp. 579–601.Wiley.

Thompson, C. E. L., Amos, C. L., Angelaki, M., Jones, T. E. R. & Binks, C. E. 2006 An evaluation of bed shear stress under turbid flows. *J. Geophys. Res.* **111**, C04008.

Thornton, E. B., Humiston, R. T. & Birkemeier, W. 1996 Bar/trough generation on a natural beach. *J. Geophys. Res.* **101** (C5), 12097–12110.

Trowbridge, J. & Young, D. 1989 Sand transport by unbroken water waves under sheet flow conditions. *J. Geophys. Res.* **94** (C8), 10971–10991.

Umlauf, L., Burchard, H. & Bolding, K. 2006 *GOTM Sourcecode and test case documentation.* Version 3.2, http://www.gotm.net, pp. 1–231.

Vanoni, V. A. 1946 Transportation of suspended sediment by water. *Trans. Am. Soc. Civ. Engng* **111**, 67–133.

Winterwerp, J. C. 2001 Stratification effects by cohesive and noncohesive sediment. *J. Geophys. Res.* **106** (C10), 22559–22574.

Winterwerp, J. C. 2006 Stratification effects by fine suspended sediment at low, medium, and very high concentrations. *J. Geophys. Res.* **111**, C05012.

Zanke, U. 1977 Berechnung der Sinkgeschwindigkeiten von Sedimenten. *Mittleilungen des Franzius-Institutes* **46**, 231–245.